Multiphoton Ion Pair Spectroscopy (MPIPS) with Ultrashort Laser Pulses for the H_2 Molecule†

André D. Bandrauk,* Deyana S. Tchitchekova, and Szczepan Chelkowski

Laboratoire de Chimie Théorique, Département de Chimie, Faculté des Sciences, Université de Sherbrooke, Sherbrooke, Québec J1K 2R1, Canada

Received: May 10, 2007; In Final Form: July 28, 2007

Time-dependent Schrödinger equation, TDSE, simulations have been performed in order to prepare and study via MPIPS the evolution of vibrational wave packets on the ion pair electronic state potentials $B''\bar{B}^1\Sigma_u^+$ and $H\bar{H}^1\Sigma_g^+$ of the H_2 molecule. Using ab initio potential surfaces and transition moments, we present two- and three-photon excitation schemes with ultrashort pulses ($\tau \leq 10$ fs) to prepare coherent superpositions of the two ion pair H^+H^- and H^-H^+ states from the doorway $B^1\Sigma_u^+$ state, which result from the strong radiative coupling between these two electronic states. The simulations are used to estimate the time evolution and recursion times of vibrational wave packets at large internuclear distances, usually not accessible by single-photon spectroscopy. Conditions for the localization of the ion pair states are proposed.

1. Introduction

Electron transfer is a fundamental and ubiquitous chemical process which occurs naturally between atoms of different nuclear charge. The simplest example is the NaI system, which is ionic in the ground state, Na^+I^-, but covalent in the first excited state, an example of electron back-transfer. Vibrational wave packet studies of the electron transfer and back-transfer have been performed in detail by Zewail by photoexcitations with short ($\tau \geq 100$ fs) pulses.[1,2] Less well-known is that ion pair states exist in the highly excited electronic states of symmetric molecules, such as H_2, as pointed out by Mulliken in 1939.[3,4] Such states have now been identified in other symmetric molecules for which high-resolution spectroscopy has led to unravelling of ion pair dissociation dynamics.[5,6]

Ion pair states of symmetric molecules usually have large equilibrium internuclear distances and cross valence states at the much shorter equilibrium distances of the latter neutral (covalent) states. Thus, highly excited electronic and vibrational states are necessary to probe the properties of ion pair states. As an example, double-resonance excitation of H_2 with extreme UV radiation has been used to observe rovibrational states of the double-well $H\bar{H}^1\Sigma_g^+$ potential at large internuclear distances of 11 au (atomic units).[7,8]

Symmetric ion pair states, such as the $B''\bar{B}^1\Sigma_u^+$ and $H\bar{H}^1\Sigma_g^+$ states, have large electronic transition moments proportional to qR, where q is the charge transfer and R the internuclear distance. This leads to strong electronic absorption bands called charge resonance bands.[3] With increasing field strengths E, as available currently with intense laser fields,[9] the radiative coupling $qR \times E$ can become larger than vibrational energies, thus leading to laser-induced avoided crossings and laser-induced molecular potentials, LIMP's.[4] At laser intensities exceeding 10^{13} W/cm^2, a new nonperturbative phenomenon, called charge resonance enhanced ionization, CREI, leads through these ion pair or charge resonance states to enhanced ionization.[10] The H^+H^- and H^-H^+ are, in fact, doorway states to intense laser field ionization[11] and lead to extreme multiphoton coupling in symmetric molecular systems.[12−14] Interest in symmetric charge-transfer states is growing also in photoinduced intramolecular electron transfer of large dimer molecular systems, where charge-separated ion pair states, P^+-P^-, are known to occur in solution.[15]

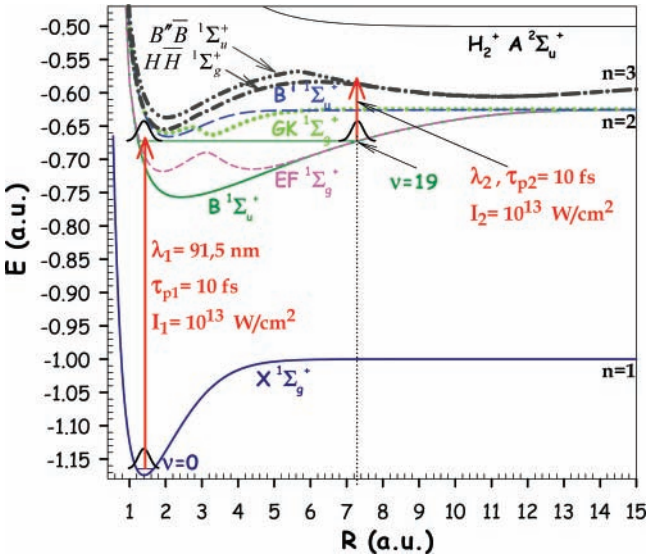

Figure 1. Potential energy curves for the seven electronic states of the H_2 molecule[17] are represented as a function of the internuclear distance (in atomic units). Also shown is the schematic pump(λ_1, I_1)−probe(λ_2, I_2) excitation process of the two ion pair states, $H\bar{H}$ and $B''\bar{B}$, via the intermediate $B^1\Sigma_u^+$ state by MPIPS.

In the present paper, we study numerically from solutions of the appropriate time-dependent Schrödinger equation, TDSE, vibrational wave packet evolution in the ion pair states $B''\bar{B}^1\Sigma_u^+$ and $H\bar{H}^1\Sigma_g^+$ corresponding to the sum of the H^+H^- and H^-H^+ ion configurations of H_2, prepared by MPIPS. In

† Part of the "Sheng Hsien Lin Festschrift".

* To whom correspondence should be addressed. Canada Research Chair—Computational Chemistry and Photonics, Université de Sherbrooke, 1500, Boul. de l'Université, J1K 2R1, Sherbrooke (Québec), Canada. E-mail: Andre.Bandrauk@USherbrooke.ca.

10.1021/jp073580w CCC: $37.00
Published on Web 08/25/2007

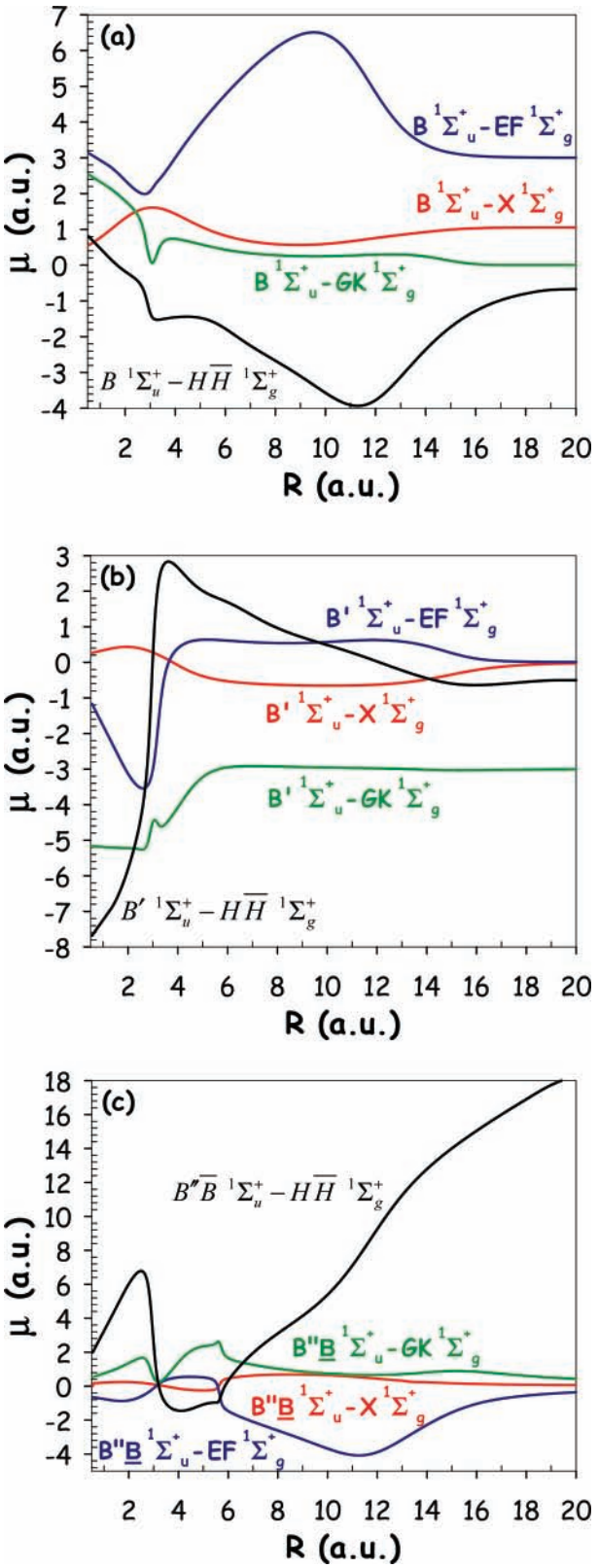

Figure 2. Transition dipole moments (in atomic units) used in the seven-electronic-states model of the H_2 molecule[18] as function of the internuclear distance (in atomic units); (a) from level $B^1\Sigma_u^+$, (b) from level $B'^1\Sigma_u^+$, and (c) from level $B''\bar{B}^1\Sigma_u^+$.

Figure 1, we illustrate seven potential surfaces and in Figure 2 the corresponding electronic transition moments used in the numerical simulations. We use numerical techniques based on split-operator methods[16] to examine the detailed time evolution of nuclear wave packets, both bound (vibrational) and continuum (dissociative), on the individual electronic states in Figure 1. We use the one-photon excited $B^1\Sigma_u^+$ state as the doorway state to pump the $H\bar{H}^1\Sigma_g^+$ (see scheme in Figure 1) by further one-photon or three-photon excitation, whereas the $B''\bar{B}^1\Sigma_u^+$ state is excited by a two-photon process from the $B^1\Sigma_u^+$ state. In this second excitation of the ion pair states, ultrashort intense pulses are used to follow the wave packet evolution and to assess the effect of the strong radiative coupling expected between the two ion pair states, $B''\bar{B}^1\Sigma_u^+$ and $H\bar{H}^1\Sigma_g^+$. Recursion times corresponding to vibrations between inner and outer turning points of the $B^1\Sigma_u^+$ potential will be shown to occur in ~40 fs. Conditions for observing vibrational wave packets on either the $B''\bar{B}^1\Sigma_u^+$ or $H\bar{H}^1\Sigma_g^+$ potentials are established. We use ab initio calculations of Wolniewicz for all potentials[17] and transition moments.[18] The long-range or large R behavior of these transition moments determines the nonperturbative effects to be expected. As an example, the $B\Sigma_u^+ \rightarrow EF\Sigma_g^+$ and $B\Sigma_u^+ \rightarrow H\bar{H}\Sigma_g^+$ transition moments vary linearly for $4 \leq R \leq 12$ au, whereas the $B''\bar{B}\Sigma_u^+ \rightarrow H\bar{H}\Sigma_g^+$ transition moment varies linearly for $R > 6$ au. These are all indications of charge-transfer effects, in particular the $B''\bar{B}\Sigma_u^+ \rightarrow H\bar{H}\Sigma_g^+$ transition moment, which varies exactly as R, a signature of the dominance of the charge-transfer or ion pair states H^+H^- and H^-H^+.[3,11,12]

2. Numerical Method

In order to study the multiphoton response of the H_2 system, we start with the general molecular Hamiltonian for the nuclear dynamics

$$\hat{H}_{mol} = \hat{K}(R) + \hat{V}_m(R) + \hat{V}_{int}(R,t) \quad (1)$$

where $\hat{K}(R)$ and $\hat{V}_m(R)$ are the proton kinetic energy operator and the molecular potentials (Figure 1). $\hat{V}_{int}(R,t)$ is the time-dependent external interaction induced by the laser pulse, which in the dipole approximation ($\lambda \gg R$, where λ is the laser pulse wavelength), can be written as

$$\hat{V}_{int}(R,t) = -\mu(R)\epsilon(t) \quad (2)$$

The $\mu(R)$ are the individual electronic transition moments illustrated in Figure 2, and $\epsilon(t)$ is the time-dependent laser field, defined in eqs 8−10. The total TDSE for the seven-potential system is (in atomic units, $\hbar = 1$ and proton mass $m_p = 1837$)

$$i\frac{\partial\Psi(R,t)}{\partial t} = [\hat{K}(R) + \hat{V}(R,t)]\Psi(R,t) \quad (3)$$

where $\hat{K} = -(1/m_p)\partial^2/\partial R^2$ and $\hat{V}(R,t) = \hat{V}_m(R) + \hat{V}_{int}(R,t)$. $\hat{V}(R,t)$ is thus a time-dependent 7×7 matrix which does not commute at different times, that is, $[\hat{V}(R,t), \hat{V}(R,t')] \neq 0$ and furthermore $[\hat{K}(R), \hat{V}(R,t)] \neq 0$. The formal solution of eq 3 is

$$\Psi(R,t+\Delta t) = \hat{T}\exp\{-i\int_t^{t+\Delta t}[\hat{K}(R) + \hat{V}(R,t)]dt\}\Psi(R,t) \quad (4)$$

$\hat{T}$ is the time-ordering operator due to the noncommutativity of the operators $\hat{K}(R)$ and $\hat{V}(R,t)$. A split-operator method is then used to approximate, to second-order accuracy,[19] the time evolution of the seven-component vector function $\Psi(R,t)$

$$\Psi(R,t+\Delta t) = \exp\left[-i\hat{K}\left(R\frac{\Delta t}{2}\right)\right]\exp\left[-i\hat{V}\left(R,t+\frac{\Delta t}{2}\right)\Delta t\right] \exp\left[-i\hat{K}\left(R\frac{\Delta t}{2}\right)\right]\Psi(R,t) + O(\Delta t^3) \quad (5)$$

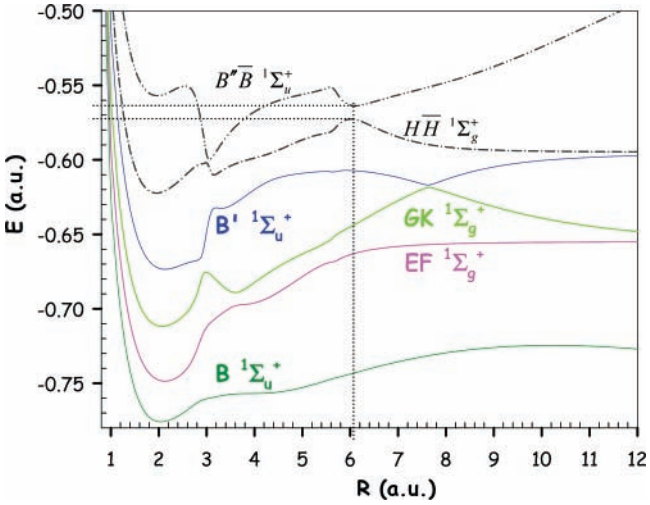

Figure 3. Diagonalized (dressed) potentials (in atomic units) as function of the internuclear distance in a static laser field $\epsilon = 1.195 \times 10^{-2}$ au ($I = 5 \times 10^{12}$ W/cm^2). An avoided crossing occurs between the two ion pair states at an internuclear distance of $R = 6.05$ au, and the corresponding energy gap between them ($\Delta E \cong 0.01$ au) is larger than typical vibrational energies for the H_2 molecule.

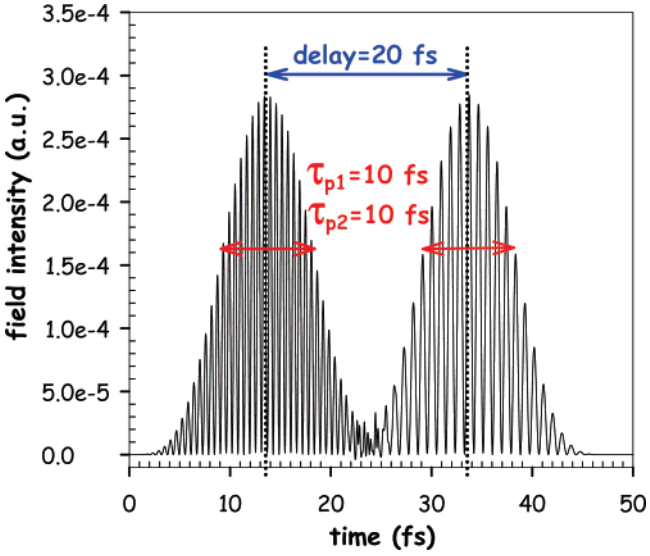

Figure 4. Laser field intensity (in au) time profile (in fs) for field parameters $I_1 = I_2 = 10^{13}$ W/cm^2, $\lambda_1 = 91.5$ and $\lambda_2 = 556$ nm, $\tau_1 = \tau_2 = 10$ fs, and fixed time delay $d_l = 20$ fs.

The kinetic energy exponentials are readily calculated by Fast Fourier Transforms (FFT).[20] The 7×7 matrix $\hat{V}(R,t)$ is nondiagonal and can be split into a time-independent diagonal part, $\hat{V}_m(R)$, and a nondiagonal time-dependent part, $\hat{V}_{int}(R,t)$. Thus, $\exp[-i\hat{V}(R,t)\Delta t]$ is factorized itself as $\exp[-i\hat{V}_m(R)\Delta t/2]\exp[-i\hat{V}_{int}(R,t)\Delta t]\exp[-i\hat{V}_m(R)\Delta t/2]$. The 7×7 matrix $\hat{V}_{int}(R,t)$ is nondiagonal and is diagonalized[19] by a unitary matrix U such that $U\hat{V}_{int}(R,t)U^+ = \hat{D}(R,t)$, where $\hat{D}(R,t)$ is a diagonal matrix and U^+ is the conjugate of U. We note that $\hat{V}_{int}(R,t) = \epsilon(t)\hat{V}_D(R)$, where $\hat{V}_D(R)$ is the purely nondiagonal dipole transition matrix, which is time-independent; therefore, it is only diagonalized once for all R. Using the above numerical procedures, the TDSE (eq 3) is integrated with a time step of $\Delta t = 0.1$ au (2.4 attoseconds) and a spatial step of $\Delta R = 0.05$ au (0.026 Å).

The TDSE (eq 3) does not include nonadiabatic couplings between electronic states since these are not known for all states in the present simulation. Such nonadiabatic (nonradiative) couplings are on the order of excited-state vibrational energies (smaller than 1000 cm^{-1} = 0.1 eV). These couplings are further slower than the laser periods, that is, 30 fs (1000 cm^{-1}) versus 2.7 fs for a 800 nm laser, and therefore can be neglected due to their slower time scales. We indicate that these field-free nonadiabatic corrections are negligible at the field intensities $10^{12} \le I \le 10^{13}$ W/cm^2 that we shall use. Thus, at $I = 10^{13}$ W/cm^2 ($\epsilon = 1.7 \times 10^{-2}$ au) and at $R \ge 3$ au, where valence electron state avoided crossings occur, as seen from the quick variations of the transition moments (Figure 2), the radiative coupling $R\epsilon \ge 0.05$ au (1.4 eV). This is considerably larger than vibrational energies so that laser-induced radiative couplings, which are included fully in the present TDSE, will dominate over field-free nonadiabatic couplings.[4] Figure 3 shows the diagonalized (dressed) potentials at a peak intensity of $I = 5 \times 10^{12}$ W/cm^2 ($\epsilon = 1.2 \times 10^{-2}$ au) and the corresponding laser-induced avoided crossings, which occur between the states at an internuclear distance of $R = 6.05$ au. We see in Figure 3 considerable radiative distortion of the molecular potentials, thus confirming the dominance of radiative couplings.

With intensities of $I > 10^{13}$ W/cm^2, we should further consider possible ionization of the bound electronic states of

Figure 1. Using the simple tunneling ionization rate for atoms at field strength ϵ[21]

$$w(t) = 4\frac{\omega_0}{\epsilon}(2I_p)^{5/2}\exp\left[-\frac{2}{3}\frac{(2I_p)^{3/2}}{\epsilon}\right] \qquad (6)$$

where ω_0 is the atomic unit rate (4×10^{16} s^{-1}) and I_p the ionization potential in atomic units, we estimate that the times for ionization, $\tau = 1/w(t)$, at peak field intensities, for example, $I = 10^{12}$, 5×10^{12}, and 10^{13} W/cm^2, are, respectively, $\tau = 3.3 \times 10^{-8}$, 7.6×10^{-14}, and 4.1×10^{-15} s. We have used for this estimate the ionization potential of H^-H^+, $I_p(H^-H^+) = I_p(H^-) + 1/R \cong 0.171$ au at $R = 7$ au, where $I_p(H^-) = 0.028$ au.[22] Actual ionization times will be larger due to reduction of the true ionization rates by inclusion of Franck−Condon factors, which are neglected in eq 6. Rotations are neglected due to the ultrashort pulse excitation, 10 fs, which cannot drive rotational transitions, which occur on picosecond time scales in H_2.

3. MPIPS: Multiphoton Ion-Pair Spectroscopy

We present numerical simulations based on the TDSE (eq 3) for the seven surfaces and their corresponding transition moments illustrated in Figures 1 and 2. To create nuclear wave packets on the $B''\bar{B}^1\Sigma_u^+$ and $H\bar{H}^1\Sigma_g^+$ ion pair states, we first use a pump laser pulse in the UV region to first excite the $B^1\Sigma_u^+$ state from the ground $X^1\Sigma_g^+$ state of H_2. A second pulse, the probe, is time-delayed with respect to the first to induce one-, two-, or three-photon transitions to the ion pair states. The pump−probe scheme is summarized as follows

$$X^1\Sigma_g^+ (v = 0) \xrightarrow{\text{pump}} B^1\Sigma_u^+ \xrightarrow{\text{probe}} H\bar{H}^1\Sigma_g^+, B''\bar{B}^1\Sigma_u^+ \qquad (7)$$

For numerical simulation of eq 2, we use a linearly polarized laser field, represented by two pulses, the pump $\epsilon_1(t)$ and the probe $\epsilon_2(t)$ laser pulses

$$\epsilon(t) = \epsilon_1(t - t_1^{tot}/2) + \epsilon_2(t - t_1^{tot}/2 - d_l) \qquad (8)$$

where $t_1^{tot}/2$ is the peak position of the pump pulse and d_l is the time delay of the probe pulse with respect to the pump pulse.

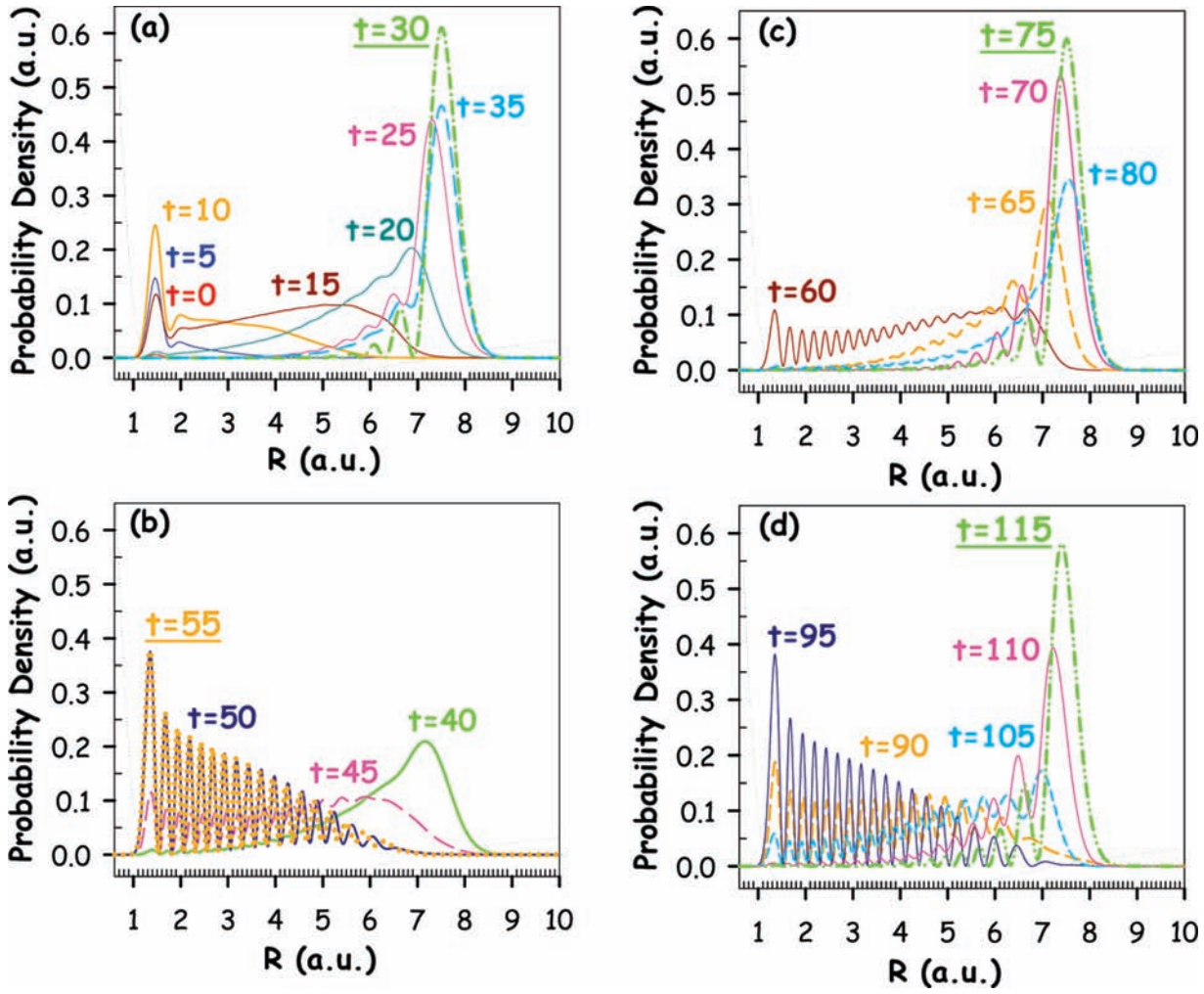

Figure 5. The nuclear probability density $|\Psi(R,t)|^2$ on the $B^1\Sigma_u^+$ state (around $v = 19$) as a function of the internuclear distance at different times. At times 30, 75, and 115 fs, the vibrational wave packet reaches the outer turning point of that potential, and its recurrence time is ~40 fs or a corresponding frequency of $\omega = 800$ cm^{-1}.

The corresponding electric fields are given by the following equations[23−25]

$$\epsilon_k(t) = -1/c(\partial A_k/\partial t) \tag{9}$$

$$A_k(t) = \begin{cases} -c\epsilon_{0,k}[\cos^2(\pi t/t_k^{tot})\sin\{\omega_k t + \varphi_k\}] & \text{for } -t_1^{tot}/2 < t < t_1^{tot}/2 \\ 0 & \text{elsewhere} \end{cases} \tag{10}$$

where $k = 1,2$; c is the speed of light, $\epsilon_{0,k}$ are the amplitudes, ω_k are the frequencies, and φ_k are the carrier-envelope phases. The forms of the pulses are chosen to satisfy the zero area theorem, $\int\epsilon(t)dt = 0$, implied by Maxwell's equations for ultrashort pulses.[9]

We have varied the field parameters in the simulations in order to obtain optimal preparation of the ion pair states. Laser pulse parameters are chosen such as to satisfy the following optimal conditions: (i) we need to reach the $R > 6-7$ au region of the $B^1\Sigma_u^+$ potential well to ensure that the $\mu(H\bar{H}-B''\bar{B})$ transition moment varies linearly with R (charge resonance effect), and (ii) we need to keep non-negligible Franck−Condon factors for the transition

$$X^1\Sigma_g^+ (v = 0) \xrightarrow{\text{pump}} B^1\Sigma_u^+$$

The best compromise between these two conditions is obtained for the $v = 19$ vibrational level of the $B^1\Sigma_u^+$ electronic state. For more clarity, we show in Figure 4 the time profile of the laser field intensity for specific parameters: time delay $d_l = 20$ fs, half-widths $\tau_1 = \tau_2 = 10$ fs, wavelengths $\lambda_1 = 91.5$ and $\lambda_2 = 556$ nm, and peak intensities $I_1 = I_2 = 10^{13}$ W/cm^2. As we will demonstrate later , the time delay d_l between the pump and probe pulses is the essential parameter for the dynamics of the ion pair states.

In order to populate the ion states through the $B^1\Sigma_u^+$ state, we use a pump frequency to access vibrational levels $v > 15$ with turning points $R > 6$ au, where the $H\bar{H}-B''\bar{B}$ transition moment is large and varies linearly with R (Figure 2c). Choosing $\omega_1 = 0.5$ au ($\lambda_1 = 91.5$ nm) with a peak intensity of $I_1 = 10^{13}$ W/cm^2 ($\epsilon_{01} = 1.7 \times 10^{-2}$ au) and a half-width of $\tau_1 = 10$ fs (the second electric field, corresponding to the probe pulse, is set equal to zero here), a one-photon resonance between $v = 0(X^1\Sigma_g^+)$ and $v = 19(B^1\Sigma_u^+)$ produces a wave packet on the $B^1\Sigma_u^+$ state whose temporal evolution is illustrated in Figure 5. The nuclear probability density $|\Psi(R,t)|^2$ is shown as a function of the internuclear distance, R, for different times, t. One sees clearly from this figure that at times 30, 75, and 115 fs, the vibrational wave packet of the $B^1\Sigma_u^+$ state around $v = 19$ is well localized at the outer turning point, $R \cong 7$ au, of that

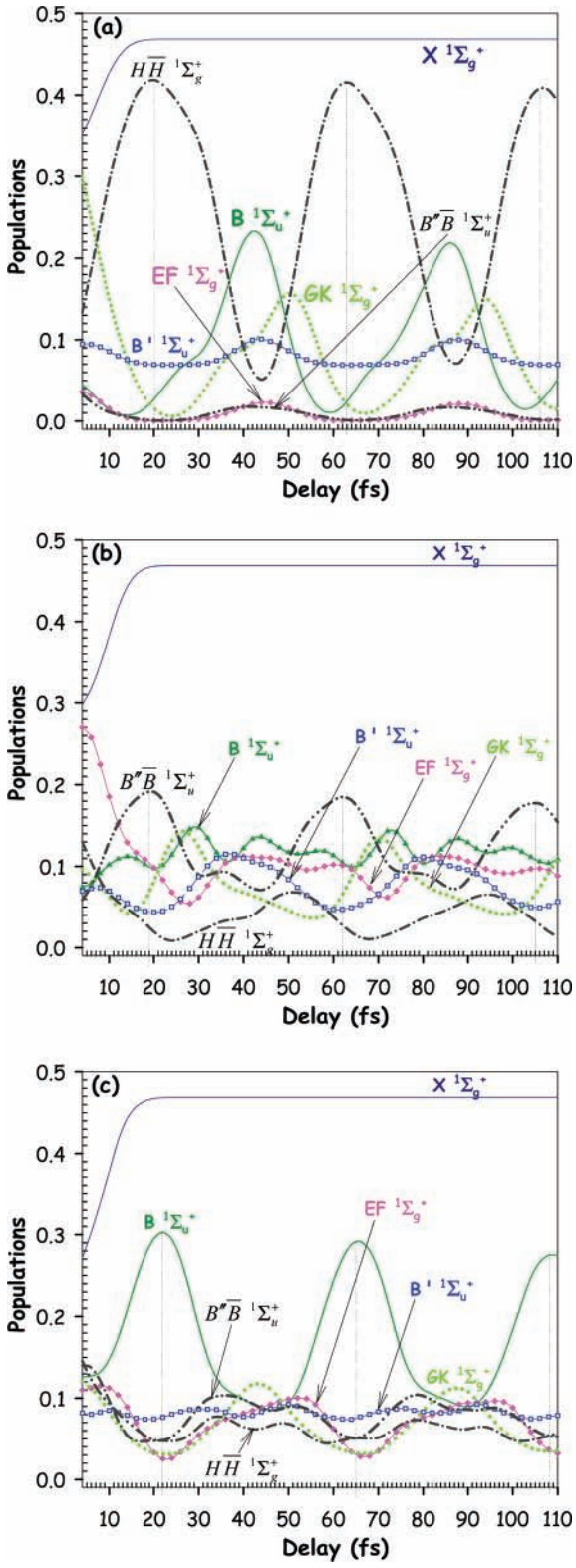

Figure 6. (a) State populations as a function of the time delay d_l (in fs) at intensities $I_1 = I_2 = 10^{13}$ W/cm^2, wavelengths $\lambda_1 = 91.5$ and $\lambda_2 = 556$ nm, and half-widths $\tau_1 = \tau_2 = 10$ fs. A maximum population of the $H\bar{H}^1\Sigma_g^+$ state is achieved for certain delays, 20, 63, and 106 fs. (b) State populations by a two-photon transition from the $B^1\Sigma_u^+$ state to the $B''\bar{B}^1\Sigma_u^+$ ion pair state at intensities $I_1 = I_2 = 10^{13}$ W/cm^2, wavelengths $\lambda_1 = 91.5$ and $\lambda_2 = 1112$ nm, and half-widths $\tau_1 = \tau_2 = 10$ fs. Periodic population transfer to the $B''\bar{B}^1\Sigma_u^+$ ionic state is achieved for delays of 19, 62, and 105 fs. (c) State populations by a three-photon transition from the $B^1\Sigma_u^+$ state to the $H\bar{H}^1\Sigma_g^+$ ion pair state at intensities $I_1 = I_2 = 10^{13}$ W/cm^2, wavelengths $\lambda_1 = 91.5$ and $\lambda_2 = 1668$ nm, and half-widths $\tau_1 = \tau_2 = 10$ fs.

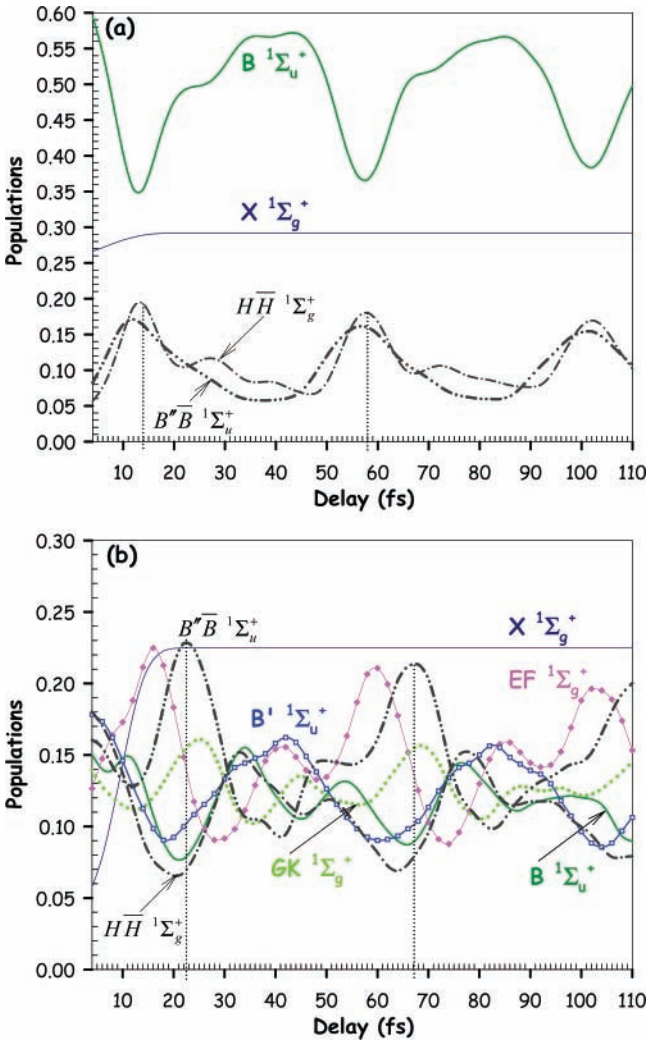

Figure 7. (a) Populations of the four electronic states as a function of the time delay (in fs). A three-photon transition ($\lambda_2 = 1668$ nm) from the $B^1\Sigma_u^+$ state to the $H\bar{H}^1\Sigma_g^+$ ion pair state is operative at laser field intensities of $I_1 = I_2 = 2 \times 10^{13}$ W/cm^2. (b) Populations of all seven electronic states at field intensities of $I_1 = I_2 = 2 \times 10^{13}$ W/cm^2 as function of the time delay (in fs) are given for comparison with (a) where only four electronic states are taken into account.

potential. The recurrence time of the wave packet is 40−45 fs or a corresponding frequency of $\omega \approx 800$ cm^{-1}.

Adding next the probe pulse with an intensity of $I_2 = 10^{13}$ W/cm^2 ($\epsilon_{02} = 1.7 \times 10^{-2}$ au), $\lambda_2 = 556$ nm, and $\tau_2 = 10$ fs, we illustrate in Figure 6a the population distributions for all seven potential surfaces as a function of the time delay d_l. The wavelength $\lambda_2 = 556$ nm induces a direct one-photon transition to the symmetric ion pair state $H\bar{H}^1\Sigma_g^+$. At an intensity of 10^{13} W/cm^2, the maximum population of this state is 42% for certain delays which have a periodicity of 43 fs, the recurrence time of the $B^1\Sigma_u^+$ wave packet (Figure 5). Figure 6a shows, in fact, that the $B^1\Sigma_u^+$ population is out of phase with the $H\bar{H}^1\Sigma_g^+$ population. Other states, such as $B''\bar{B}^1\Sigma_u^+$ and $EF^1\Sigma_g^+$, follow the $B^1\Sigma_u^+$ state so that at maximum excitation of the $H\bar{H}$ ion pair state, one has an ∼45% population of the $X^1\Sigma_g^+$ and $H\bar{H}^1\Sigma_g^+$ states in the molecule. It is to be noted that at $\lambda_2 = 556$ nm, the population of the other ion pair state, $B''\bar{B}^1\Sigma_u^+$, is well below 5% since the $H\bar{H}$ and $B''\bar{B}$ are coupled radiatively by one-photon transitions, but these transitions are nonresonant and lead to little population transfer.[10]

We next examine two- and three-photon transitions to the ion pair states by choosing wavelengths $\lambda_2 = 1112$ and 1668 nm successively, that is, by doubling and tripling the probe wavelength. The doubled wavelength will induce direct two-photon transitions from the $B^1\Sigma_u^+$ state to the other ion pair state of the same symmetry, the $B''\bar{B}^1\Sigma_u^+$. This state however may couple radiatively with the symmetric $H\bar{H}^1\Sigma_g^+$ state during this transition. The tripled wavelength will allow one to study a three-photon transition from the $B^1\Sigma_u^+$ state to the symmetric ion pair state $H\bar{H}^1\Sigma_g^+$, which can strongly couple radiatively to the antisymmetric ion pair state $B''\bar{B}^1\Sigma_u^+$ due to the large transition moment, varying with R, between these two. Results of the simulations from the TDSE (eq 3) are shown in Figure 6b and c. The populations by two-photon excitation of the $B''\bar{B}^1\Sigma_u^+$ state (Figure 6b) and by three-photon excitation of the $H\bar{H}^1\Sigma_g^+$ state (Figure 6c) are now less than the one-photon (resonant) excitation probability of $H\bar{H}^1\Sigma_g^+$ (Figure 6a), that is, it is more difficult to isolate the two ion pair states from others via two- and three-photon transitions out of the $B^1\Sigma_u^+$ state. Thus, in Figure 6b, a 20% periodic (with same period of 43 fs as in 6a) population transfer to the $B''\bar{B}^1\Sigma_u^+$ ionic state is achieved at the outer turning point of the $B^1\Sigma_u^+$ state. Little transfer to the $H\bar{H}$ symmetric ion pair state occurs as the wavelength $\lambda_2 = 1112$ nm corresponds to a photon energy larger than the energy separation between the two ion pair states. Of note is that in Figure 6c, where a three-photon transition between the $B^1\Sigma_u^+$ and $H\bar{H}^1\Sigma_g^+$ states is operative, the populations of the two ion pair states, $B''\bar{B}^1\Sigma_u^+$ and $H\bar{H}^1\Sigma_g^+$, are nearly equal. This is indicative of localization of the charge transfer into either the left configuration H^-H^+ or the right configuration H^+H^- separately. Thus, the larger wavelength $\lambda_2 = 1668$ nm or lower frequency ω_2 creates a coherent superposition of the delocalized ion pair states, $\Psi(B''\bar{B}) \pm \Psi(H\bar{H})$, leading to a more localized charge transfer H^-H^+ or H^+H^-.

The influence of the strong radiative coupling between the two ion pair states $B''\bar{B}^1\Sigma_u^+$ and $H\bar{H}^1\Sigma_g^+$ leading to ion pair state localization is confirmed in a calculation at higher intensity, illustrated in Figure 7, where we compare a four-electronic-state simulation (including $X^1\Sigma_g^+$, $B^1\Sigma_u^+$, $H\bar{H}^1\Sigma_g^+$, and $B''\bar{B}^1\Sigma_u^+$ states), Figure 7a, to the full seven-state simulation, Figure 7b. Thus, at equal pump−probe pulse intensities $I_1 = I_2 = 2 \times 10^{13}$ W/cm^2, wavelengths $\lambda_1 = 91.5$ and $\lambda_2 = 1668$ nm, and half-widths $\tau_1 = \tau_2 = 10$ fs, we obtain equal symmetric $H\bar{H}$ and antisymmetric $B''\bar{B}$ ion pair state populations by omitting the symmetric EF and GK double-well states and the antisymmetric B′ state of H_2 (Figure 7a). Comparing Figure 7a and b, one sees that the intermediate electronic states (EF, GK, and B′) inhibit the radiative coupling at high intensities.

Conclusion

Ion pair states in symmetric molecules have large electronic transition moments, leading to intense charge resonance (transfer) absorptions. With intense lasers, these states are doorway states to enhanced ionization. We have performed numerical experiments using accurate potentials and electronic transition moments in the TDSE (eq 3) to investigate the feasibility of preparing vibrational wave packets in the ion pair states, the symmetric $H\bar{H}^1\Sigma_g^+$ and antisymmetric $B''\bar{B}^1\Sigma_u^+$ states of H_2, via multiphoton ion pair spectroscopy, MPIPS. Using single-UV-photon excitation of the high vibrational levels ($v \geq 19$) of the $B^1\Sigma_u^+$ state with ultrashort ($\tau \sim 10$ fs) pump pulses allows for efficient preparation of the ion pair states from the large-distance ($R > 7$ au) turning points of the $B^1\Sigma_u^+$ wave packets. One-, two-, and three-photon ultrashort pulse excitations out of the $B^1\Sigma_u^+$ state into the ion pair states was shown to lead to efficient preparation of $H\bar{H}$ and $B''\bar{B}$ ion pair vibrational wave packets by one- and two-photon absorption, respectively, and with little radiative coupling between the two. Three-photon excitation from the $B^1\Sigma_u^+$ state leads to nearly equal populations of the $H\bar{H}$ and $B''\bar{B}$ ion pair states, allied with simultaneous excitation of other electronic states due to strong radiative couplings between all electronic states with ultrashort ($\tau \sim 10$ fs) intense ($I \sim 10^{13}$ W/cm^2) pulses of low frequency ($\lambda_2 = 1668$ nm). Since such ion pair states exist at large internuclear distances and are separated by small energies, the coherent superposition by MPIPS with intense ultrashort pulses should lead, in principle, to charge localization of the ion pair states in symmetric molecules. The study of the temporal evolution of such localized ion pair states prepared by MPIPS would provide new methods of characterizing charge-transfer processes in symmetric molecules. The present numerical study shows that for H_2, high intensities and low frequencies are necessary to prepare such localized states (see Figure 7a) whose lifetimes in H_2 are on the femtosecond time scale due to low ionization potentials. Furthermore, overlapping absorptions such as $X^1\Sigma_g^+ \rightarrow B^1\Sigma_u^+$ and $X^1\Sigma_g^+ \rightarrow B'^1\Sigma_u^+$ (Figure 1) can inhibit equal population of the ion pair states (Figure 7b). We conclude that localization of ion pair states should be more easily achievable and measurable in highly charged molecular ions,[14] where higher ionization potentials will lead to much larger lifetimes in intense fields and larger energy separations of excited-state potentials.

Acknowledgment. We thank CIPI, the Canadian Institute for Photonics Innovation, for financial support of this project and also Professor S. H. Lin for "illuminating" discussions on charge-transfer processes in molecules. Finally, we thank Professor L. Wolniewicz for his generosity in supplying rare transition moments.

References and Notes

(1) (a) Rose, T. S.; Rosker, M. J.; Zewail, A. H. *J. Chem. Phys.* **1988**, *88*, 6672. (b) Rose, T. S.; Rosker, M. J.; Zewail, A. H. *J. Chem. Phys.* **1989**, *91*, 7415.

(2) Cong, P.; Roberts, G.; Herek, J. L.; Mohktari, A.; Zewail, A. H. *J. Phys. Chem.* **1996**, *100*, 7382.

(3) Mulliken, R. S. *J. Chem. Phys.* **1939**, *7*, 20.

(4) Bandrauk, A. D. *Molecules in Laser Fields*; Marcel Dekker Publications, Inc.: New York, 1994.

(5) Martin, J. D. D.; Hepburn, J. W. *Phys. Rev. Lett.* **1997**, *79*, 3154.

(6) Suits, A. G.; Hepburn, J. W. *Annu. Rev. Phys. Chem.* **2006**, *57*, 431.

(7) Reinhold, E.; Hogervorst, W.; Ubachs, W. *Phys. Rev. Lett.* **1997**, *78*, 2543.

(8) de Lange, A.; Hogervorst, W.; Ubachs, W.; Wolniewicz, L. *Phys. Rev. Lett.* **2001**, *86*, 2988.

(9) Brabec, T.; Krausz, F. *Rev. Mod. Phys.* **2000**, *72*, 545.

(10) (a) Zuo, T.; Bandrauk, A. D. *Phys. Rev. A* **1995**, *52*, 2511, (b) Zuo, T.; Bandrauk, A. D. *Phys. Rev. A* **1996**, *54*, 3254.

(11) Kawata, I.; Kono, H.; Fujimura, Y.; Bandrauk, A. D. *Phys. Rev. A* **2000**, *62*, 031401.

(12) Kawata, I.; Kono, H.; Bandrauk, A. D. *Phys. Rev. A* **2001**, *64*, 043411.

(13) Harumiya, K.; Kono, H.; Fujimura, Y.; Kawata, I.; Bandrauk, A. D. *Phys. Rev. A* **2002**, *66*, 043403.

(14) Gibson, G. N. *Phys. Rev. A* **2003**, *67*, 043401.

(15) Holman, M. W.; Yan, P.; Adams, D. M.; Westenhoff, S.; Silva, C. *J. Phys. Chem. A* **2005**, *109*, 8548.

(16) Bandrauk, A. D.; Dehghanian, E.; Lu, H. Z. *Chem. Phys. Lett.* **2006**, *419*, 346.

(17) (a) Wolniewicz, L. *J. Chem. Phys*. **1983**, *78*, 6173. (b) Wolniewicz, L. *J. Chem. Phys.* **1995**, *103*, 1792.

(18) Wolniewicz, L. http://www.fizyka.umk.pl/ftp/publications/ifiz/luwo/.
(19) Bandrauk, A. D.; Shen, H. *J. Chem. Phys.* **1993**, *99*, 1185.
(20) Press, W. H.; Teukolsky, S. A.; Vetterling, W. T.; Flannery, B. P. *Numerical Recipes in Fortran*, 2nd ed.; Cambridge University Press: New York, 1992.
(21) Dietrich, P.; Corkum, P. B. *J. Chem. Phys.* **1992**, *97*, 3187.
(22) Pekeris, C. L. *Phys. Rev.* **1958**, *112*, 1649.
(23) Chelkowski, S.; Bandrauk, A. D. *Phys. Rev. A* **2002**, *65*, 061802.
(24) Bandrauk, A. D.; Chelkowski, S.; Shon, N. H. *Phys. Rev. Lett.* **2002**, *89*, 283903.
(25) Chelkowski, S.; Bandrauk, A. D.; Apolonski, A. *Phys. Rev. A* **2004**, *70*, 013815.